Continuous Switching Control of an Input-Delayed Antagonistic Muscle Pair During Functional Electrical Stimulation

Ziyue Sun, Tianyi Qiu, Ashwin Iyer, Brad E. Dicianno, Nitin Sharma

Abstract—Existing controllers for functional electrical stimulation (FES) of upper-limb muscles were initially designed to assist unilateral movements and may not be readily applicable to assist antagonistic muscle movements. Further, it is yet unclear if electromechanical delays (EMD) are present during co-activation of muscles. In this paper, a robust controller is designed to facilitate FES of an antagonistic muscle pair during elbow flexion and extension. The controller uses a continuous switching law that maps a joint angle error to control the antagonistic muscle pair. Further, the controller compensates for EMDs in the antagonistic muscle pair. A Lyapunov stability analysis yields uniformly ultimately bounded tracking for the human limb joint. The experimental results on four participants without disabilities indicate that the controller is robust and effective in switching between antagonistic muscles. A separate set of experiments also showed that EMDs are indeed present in the co-activated muscle pair. The designed controller compensates for the EMDs and statistically improves root mean square error, compared to a traditional linear controller with no EMD compensation. The proposed controller can be generalized to assist FES-elicited tasks that involve a weak antagonistic muscle pair.

Index Terms—Neuromuscular stimulation, Delay systems

I. INTRODUCTION

Spinal cord injury (SCI) results in loss of muscle strength at and below the level of the spinal lesion. About 17,730 new SCI cases are reported each year in the US since 2019 [1]. Approximately 60% of these cases resulted in incomplete or complete tetraplegia from SCI. Functional electrical stimulation (FES), which is an external application of electrical currents via surface or invasive electrodes to elicit desired muscle contractions, is commonly prescribed to recover lost muscle function and/or strength in individuals who have such conditions [2]. FES enables grasping and reaching motions in people with tetraplegia who may have completely absent arm function [3], [4]. Furthermore, due to its ability to effect neuroplasticity, it promotes functional recovery in people undergoing an FES-based rehabilitation therapy [5].

Ziyue Sun is at DiDi Labs, Mountain View, CA 94043. Email: ziyue-sun@didiglobal.com. Ashwin Iyer and Nitin Sharma are in the UNC/NCSU Joint Department of Biomedical Engineering, Raleigh, NC 27695. Emails: {aiyer3, nsharma23} @nesu.edu. Tianyi Qiu is at Guangzhou Automobile Group Research and Development Center, Guangzhou, Guangdong, China, postal code: 511434. Email:qiutianyi@gacrnd.com. Brad E. Dicianno is in the Department of Physical Medicine and Rehabilitation, School of Medicine, University of Pittsburgh, Pittsburgh, PA 15213. Email: dicianno@pitt.edu. This work was funded by National Science Foundation award number 1511139. Any opinions, findings, and conclusions or recommendations expressed in this material are those of the author(s) and do not necessarily reflect the views of the National Science Foundation.

The main objective of closed-loop control of FES is to accurately deliver desired assistance or provide precise dosage of rehabilitative training. However, due to nonlinear and uncertain muscle dynamics, it is often difficult to obtain robust performance with linear or simple control methods [6]–[8]. Nonlinear control methods have also been shown to provide a superior performance [4], [9]–[11], robustness to parametric uncertainties [9], [10], and the ability to compensate for timevarying phenomena such as muscle fatigue [12]. More recently, the issue of electromechanical delay (EMD) during FES control has been addressed to improve control performance and ensure stability during FES control [13]–[15].

EMD is the time lag between the electrical excitation and the force development in a muscle, and is often modeled as an input delay in the musculoskeletal dynamics [14], [16]-[19] Unlike deadzone, which is a recruitment characteristic [20], EMD is a characteristic of temporal dynamics of the recruited motor units. EMD is mainly due to the delays from the chemical reactions and calcium release and finite conduction velocities of the action potential in the membrane system [16]. A deadzone would also cause a delayed muscle response, especially if the stimulation intensity is below a deadzone threshold but increasing. However, when stimulation is chosen above the threshold that recruits the first motor units, EMD effects can also be observed. Because input delays can cause performance degradation and system instability [21], compensating for EMD is relevant for high-performance closed-loop control design.

Recently, a robust compensation control method was developed for an uncertain input delayed system with additive disturbances [14]. The control method suggests a PD/PID controller can be augmented with a delay compensation term that contains a finite integral of past control values to transform the delayed system into a delay-free system. These modified PD/PID controllers were extended to compensate for a known EMD during FES [13], [14], [18]. Further improvements of these control designs in [15], [22] provided a capability to compensate for unknown varying EMD. However, these controllers facilitate unidirectional limb movements; i.e., only quadriceps muscles were stimulated through a single FES channel to extend the knee. The antagonist muscles (hamstrings in this case) were not stimulated. Instead the leg was lowered by a controlled reduction in FES of the quadriceps muscles, allowing gravity to help bring the leg back towards the equilibrium position. However, in a standing position or during a gait cycle, producing knee flexion and extension

would require controlled stimulation of both hamstrings and quadriceps (antagonistic pair).

Similarly, upper-limb movements such as elbow or wrist flexion and extension would require FES of antagonistic muscle pairs (e.g., biceps and triceps). Usually, persons with C5/C6 SCI have a weak to strong voluntary control of elbow flexion control but lack the ability to control elbow extension [23]. In an akin study on persons with stroke, the stimulation was applied to triceps and anterior-deltoids muscles to assist elbow extension [24]–[27]. However, FES controllers to assist people with SCI who lack the ability to voluntarily control both the elbow flexion and extension do not exist. Because the controllers in [24]–[27] were originally designed to assist unilateral movements and may not be easily applicable to assist in bilateral elbow movements, we were motivated to design an FES controller capable of antagonistic muscle control.

In general, antagonistic muscle control employs cocontraction of the muscles. Choosing co-contraction of antagonistic muscles is certainly useful in some applications as it could be used to induce desired joint impedance via FES. In [11], [28], [29] co-activating stimulation strategies were mainly designed to modulate joint impedance during regulation of wrist or elbow angle. However, using a coactivation strategy may cause an early onset of muscle fatigue. A low stimulation intensity level co-contraction strategy may sustain long duration of limb regulation but its use during high performance limb tracking is unclear. Instead, a switched strategy that alternates between antagonistic muscles may be more beneficial for limb tracking. In [30], an ad-hoc ON/OFF switching signal was designed to control the quadriceps based on a switching curve that is a function of the knee angle. In [31], [32], cadence-based switching control algorithms were designed for quadriceps, hamstrings, and gluteal muscles during FES cycling. While both co-activation and switched strategies have respective advantages, neither of these designs have considered EMD in the design.

This paper, for the first time, develops and validates a continuously switched strategy to alternately stimulate the biceps and triceps muscles for elbow regulation and tracking. The key contribution of this paper is the design of a continuous switched mapping between the antagonistic muscle stimulation and position tracking error. Further, a proportional derivative (PD)-type closed-loop controller with a delay compensation (DC) term deals with EMDs in the antagonistic muscle pair. Unlike previous controllers that produce joint flexion with the help of gravity [13], [14], [33] or controlled by correctional forces such as robot arms [24], [27], the developed controller will flex and extend a joint by stimulating agonist and antagonist muscles. The controller is designed to smoothly transition between the stimulation of the antagonist muscles and can be made arbitrarily fast or slow by adjusting the control gains. The work substantially extends our preliminary work in [34] with an improved switching signal design and addition of experimental validation on four human participants without disabilities. The proposed controller is also compared with a classical PD controller with an adhoc switching law. Parametric uncertainty and additive bounded disturbance were included in the dynamics for the control development and subsequent stability analysis. Lyapunov Krasovskii (LK) functionals were constructed to cancel the delay terms. The associated Lyapunov-based stability analysis proved semiglobal uniformly ultimately bounded tracking.

II. DYNAMIC MODEL OF UPPER LIMB WITH GRAVITY COMPENSATION

The uncertain nonlinear musculoskeletal dynamics are modeled similar to [9], and are defined as

$$M_I(\ddot{q}) + M_e(q) + M_v(\dot{q}) + d(t) = T_1(t - \tau) - T_2(t - \tau)$$
 (1)

where $M_I(\ddot{q}) \in \mathbb{R}$ denotes the inertial force about the joint, and $M_e(q) \in \mathbb{R}$ denotes the elastic effects due to joint stiffness. $M_v(\dot{q}) \in \mathbb{R}$ denotes the viscous effects from damping in the musculoskeletal system. In (1), $d(t) \in \mathbb{R}$ represents any bounded unknown disturbance and/or unmodeled dynamics, and $T_1(t-\tau) \in \mathbb{R}$ denotes torque produced due to joint extension while $T_2(t-\tau) \in \mathbb{R}$ denotes torque produced due to joint flexion. $\tau \in \mathbb{R}^+$ denotes the constant EMD value.

The inertial effects in (1) are modeled as

$$M_I(\ddot{q}) \triangleq J\ddot{q},$$
 (2)

where $J \in \mathbb{R}^+$ is the moment of inertia of the limb. The elastic effects due to joint stiffness are modeled as

$$M_e(q) \triangleq k_1 (\exp(-k_2 q)) (q - k_3),$$
 (3)

where $k_1, k_2, k_3 \in \mathbb{R}^+$ are unknown parameters.

$$M_v(\dot{q}) \triangleq B_1 \tanh(-B_2 \dot{q}) + B_3 \dot{q},\tag{4}$$

 $B_1, B_2, B_3 \in \mathbb{R}^+$ are unknown coefficients and $q, \dot{q}, \ddot{q} \in \mathbb{R}$ are the respective angular position, velocity, and acceleration of the limb.

The torque produced for extension/flexion is related to the musculotendon force generated by FES and is defined as

$$T_i(t-\tau) \triangleq \varsigma_i(q) F_{T_i}(q, \dot{q}, u_i), \ i = 1, 2, \tag{5}$$

where $\varsigma_i(q) \in \mathbb{R}$ is the positive moment arm for the corresponding muscle of the limb and $F_{T,i}(q,\dot{q},u_i) \in \mathbb{R}$ is the musculotendon force generated by the stimulated muscle. The musculotendon force $F_{T,i} \in \mathbb{R}$ in (5) is defined as

$$F_{T,i}(q, \dot{q}, u_i) \triangleq \eta_i(q, \dot{q})u_i(t - \tau), \ i = 1, 2,$$
 (6)

where $\eta_i(q,\dot{q}) \in \mathbb{R}^+$, i=1,2 denotes an unknown nonlinear function of the force-length/force-velocity relationship, and $u_i(t-\tau) \in \mathbb{R}$ is the normalized stimulation input with EMD. The unknown functions in the active dynamics of the muscles are grouped in $\Omega_i \in \mathbb{R}$ as

$$\Omega_i \triangleq \varsigma_i(q)\eta_i(q,\dot{q}), \ i = 1, 2.$$
 (7)

The normalized stimulation input, $u_i(t)$, is represented by a piecewise linear muscle recruitment function [16], defined as

$$u_i(t) = \begin{cases} 0, & v_i(t) \le V_{ithresh} \\ \frac{v_i(t)}{V_{isat} - V_{ithresh}}, & V_{ithresh} < v_i(t) < V_{isat}, \\ 1, & v_i(t) \ge V_{isat} \end{cases}$$
(8)

where $V_{ithresh}$, $V_{isat} \in \mathbb{R}^+$, i=1,2 are the threshold and saturation constants. As both stimulation intensity and pulse width can be used to increase the muscle recruitment, the stimulation input is generalized to represent either the stimulation intensity (i.e. voltage in the voltage modulation case or current amplitude in the current modulation case) or the pulse width.

The following assumptions and notation were made for the control development and stability analysis.

Assumption 1: Signals q and \dot{q} denote the generalized position and velocity and are measurable.

Assumption 2: The nonlinear functions $\eta_i(q,\dot{q})$ and moment arm $\varsigma_i(q)$ are non-zero, positive, bounded functions, and their first time derivatives exist and are continuous and bounded based on the data. As defined in [35], the moment arm is a continuously differentiable, positive, and bounded function of q(t) with a bounded first time derivative. The uncertain nonlinear function $\eta_i(q,\dot{q})$ represents the muscle force–length and muscle force-velocity relationships. Based on the definitions of these relationships in [9], [12], [36], [37], $\eta_i(q,\dot{q})$ can be assumed as continuously differentiable, non-zero, positive, and bounded functions. Thus Ω_i in (7) is also non-zero, positive bounded and its first time derivative exists, is bounded and continuous. It can be bounded as

$$\Omega_i \le \zeta_{\Omega_i}, \ i = 1, 2 \tag{9}$$

where $\zeta_{\Omega_i} \in \mathbb{R}^+$ is a constant.

Assumption 3: The EMD, denoted by τ , is assumed to be a known constant. Factors that may cause it to be a time-varying phenomenon such as fatigue [38] are ignored. Similarly, the EMD in the opposing muscles could be different, but upper bounded. For easing the control development and the stability analysis of the proposed controller, we assume that the EMD values in the antagonistic muscles are same. Also see Remark 1.

Assumption 4: The desired trajectory and its time derivatives q_d , \dot{q}_d , $\ddot{q}_d \in \mathbb{R}$ are bounded and continuous.

Notation: A delayed state in the subsequent control development and analysis is denoted as $x(t-\tau)$ or as x_{τ} while a non-delayed state is denoted as x(t) or as x. Any term, X, multiplied by the inverse of another term, B, is denoted as a subscript (i.e., X_B).

The dynamic model in Eqs. (1)-(8) is represented by an input delayed piecewise linear muscle recruitment curve whose normalized stimulation variable drives the second order musculoskeletal differential equation. Instead of an input delayed piecewise linear muscle recruitment curve, other models also exist for mapping static muscle recruitment curve; e.g., modified Hill Huxley models [39], [40], Hammerstein models [26], and recently logistic function [11]. The piecewise linear function used in the paper indeed captures the static muscle recruitment and allows one to design a controller that accounts for stimulation threshold and EMD.

Usually, the muscle recruitment function is cascaded to a first order muscle activation dynamics. In the above model, we neglected the first order muscle activation dynamics that cascades to the second order musculoskeletal dynamics. However, in our recent work [18] we presented a control design of a single muscle actuated FES control that considers both the first order muscle activation dynamics and the secondorder musculoskeletal dynamics. The approach in [18] uses dynamic surface control design to compensate for EMD for the third order musculoskeletal dynamics. For the sake of a less complex control development, the muscle activation dynamics was neglected and the control design follows second-order musculoskeletal dynamics of the input delayed antagonistic muscles. Please note that muscle activation dynamics has been ignored in earlier works as well; e.g., see work in [41], where direct muscle activation levels (ignored the first order dynamics) were designed for optimal control formulation.

Overall, our model representation allows control development and analysis using the Lyapunov stability approach, and especially enable the use of LK functionals to design an input delay compensation term. We also feel that using the approach in our previous work [18], the results in our current work can be extended in the future for a third order muscle model.

III. CONTROL DEVELOPMENT

A. Control objective

The control objective is to force the limb angle, q(t), to track a bounded desired trajectory, $q_d(t)$. Therefore, the position tracking error, $e_1(t) \in \mathbb{R}$, and auxiliary tracking error, $e_2(t) \in \mathbb{R}$, are defined as

$$e_1(t) \triangleq q_d - q,\tag{10}$$

$$e_2(t) \triangleq \dot{e}_1 + \alpha e_1 - \beta e_z,\tag{11}$$

where α , $\beta \in \mathbb{R}^+$ are control gains. The auxiliary signal, $e_z \in \mathbb{R}$, for the EMD compensation is defined as

$$e_z(t) = \int_{t-\tau}^t v(\theta) d\theta, \qquad (12)$$

Based on these tracking error signals, below we introduce the controller for the EMD compensation and continuous switched control between the antagonistic muscles.

B. Controller and Switched Mapping

The controller denoted by $v(t) \in \mathbb{R}$ is defined as

$$v(t) = Ke_2, \tag{13}$$

where $K \in \mathbb{R}^+$ is a known constant control gain and is decomposed by

$$K = K_1 + K_2 + K_3 \tag{14}$$

where $K_1, K_2, K_3 \in \mathbb{R}^+$ are positive constants designed for the stability analysis.

Next, we introduce two switching signal operators to smoothly transition between the stimulation of the flexor and extensor muscles. The switching operators $S_1(e_2): \mathbb{R} \to$

[0, 1] and $S_2(e_2): \mathbb{R} \to [-1, 0]$ that map the input error signal $e_2(t)$ to the muscle choice are defined as

$$S_1(e_2) \triangleq \frac{1 + \tanh(\kappa e_2)}{2},$$

$$S_2(e_2) \triangleq -\frac{1 - \tanh(\kappa e_2)}{2},$$
(15)

where $\kappa \in \mathbb{R}^+$ is a control gain that determines the transition

To ease in the control development, we introduce following definitions to consider the stimulation input and the recruitment characteristic in (8). The stimulation inputs to the triceps muscle $v_1(t) \in \mathbb{R}^+$ and the biceps muscle $v_2(t) \in \mathbb{R}^+$ are allocated via the switching signals as

$$v_1 \triangleq S_1 v + V_{1thresh},$$

$$v_2 \triangleq S_2 v + V_{2thresh},$$
(16)

Thus, using the definition of the normalized simulation (8), $u_i \in \mathbb{R}^+, i = 1, 2$, can be expressed as

$$u_{i} = \begin{cases} 0, & v_{i} \leq V_{ithresh} \\ \frac{S_{i}v_{i}}{V_{isat} - V_{ithresh}}, & V_{ithresh} < v_{i} < V_{isat}, \\ 1, & v_{i} \geq V_{isat} \end{cases}$$
(17)

The control block diagram is shown in Fig.1.

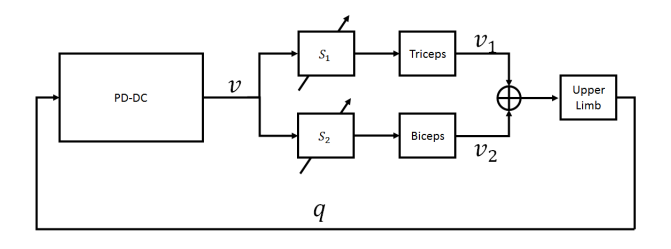


Figure 1. Block diagram of control algorithm. The PD-DC controller gives a control input v(t) in (13) and it is allocated to biceps (as v_2 in (16)) and triceps (as v_1 in (16)) muscles based on the switching function S_1 and S_2 .

C. Open Loop Error Development

After multiplying the time derivative of (11) with the moment of inertia, J, in (2), substituting the dynamics in (1), and using (6) and (7), the open loop error dynamics is expressed as

$$J\dot{e}_{2} = J\ddot{q}_{d} + M_{e} + M_{v} - \Omega_{1}u_{1\tau} + \Omega_{2}u_{2\tau}$$

$$+ d + J\alpha\dot{e}_{1} - J\beta(v - v_{\tau}).$$
(18)

By substituting (17), the (18) can be written as

$$J\dot{e}_{2} = J\ddot{q}_{d} + M_{e} + M_{v} + d - v_{\tau}\Omega$$
$$+J\alpha\dot{e}_{1} - J\beta (v - v_{\tau})$$
(19)

where $\Omega \in \mathbb{R}^+$ is defined as

$$\Omega \triangleq \frac{\Omega_1 S_{1\tau}}{V_{1sat} - V_{1thresh}} - \frac{\Omega_2 S_{2\tau}}{V_{2sat} - V_{2thresh}}, \tag{20}$$

and can be bounded as $0 < \Omega < \overline{\Omega}$. Thus, dividing the open loop error dynamics by Ω ,

$$J_{\Omega}\dot{e}_{2} = J_{\Omega}\ddot{q}_{d} + M_{e\Omega} + M_{v\Omega} + d_{\Omega} - v_{\tau}$$

$$+ J_{\Omega}\alpha\dot{e}_{1} - J_{\Omega}\beta\left(v - v_{\tau}\right)$$
(21)

where

$$J_{\Omega} = \frac{J}{\Omega}, \quad M_{e\Omega} = \frac{M_e}{\Omega}, \quad M_{v\Omega} = \frac{M_v}{\Omega}, \quad d_{\Omega} = \frac{d}{\Omega}.$$

$$J_1 \le J_{\Omega} \le J_2. \tag{22}$$

To facilitate the subsequent stability analysis, the error between β and J_{Ω}^{-1} is defined by

$$\xi = \beta - \frac{\Omega}{I},\tag{23}$$

where $\xi \in \mathbb{R}^+$ satisfies the following:

$$|\xi| \le \bar{\xi} \tag{24}$$

and $\bar{\xi} \in \mathbb{R}^+$ is a known constant. (21) can be expressed as $J_0 \dot{e}_2 = I^{-2} + I^{-2}$

$$J_{\Omega}\dot{e}_{2} = J_{\Omega}\ddot{q}_{d} + M_{e\Omega} + M_{v\Omega} + d_{\Omega} - v + J_{\Omega}\alpha\dot{e}_{1} - J_{\Omega}\xi\left(v - v_{\tau}\right)$$
(25)

D. Closed Loop Error Development

After using the control input (13), the closed loop error system can be written as

$$J_{\Omega}\dot{e}_{2} = -\frac{1}{2}\dot{J}_{\Omega}e_{2} + \bar{\psi} + \tilde{\psi} - e_{1} - KJ_{\Omega}\xi\left(e_{2} - e_{2\tau}\right) - Ke_{2},$$
(26)

where the following auxiliary signals as ψ (e_1 , e_2 , t, τ), $\bar{\psi}\left(q,\,\dot{q},\,q_d,\,\dot{q}_d,\,\ddot{q}_d,\,t\right)\in\mathbb{R}$ are used

$$\tilde{\psi} = \psi - \psi_d, \qquad \bar{\psi} \triangleq \psi_d + d_{\Omega}.$$
 (27)

$$\psi \triangleq \frac{1}{2}\dot{J}_{\Omega}e_{2} + J_{\Omega}\ddot{q}_{d} + M_{e\Omega} + M_{v\Omega} + J_{\Omega}\alpha\dot{e}_{1} + e_{1},$$

$$\psi_{d} \triangleq J_{\Omega}\ddot{q}_{d} + M_{e\Omega} + M_{v\Omega},$$
(28)

By applying the Mean Value Theorem, $\psi\left(e_{1},\,e_{2},\,,t,\, au\right)$ can be upper bounded by state-dependent terms as

$$\left|\tilde{\psi}\right| \le \rho\left(\|z\|\right)\|z\|\,,\tag{29}$$

and $\rho(||z||) \in \mathbb{R}$ is a positive, globally invertible nondecreasing function and $z \in \mathbb{R}^3$ is defined as

$$z(t) \triangleq \left[e_1, \, e_2, \, e_z \right]^T. \tag{30}$$

The second auxiliary signal, $\bar{\psi}(q, \dot{q}, q_d, \dot{q}_d, \ddot{q}_d, t)$, can be upper bounded as

$$|\bar{\psi}| \le \zeta_S,\tag{31}$$

where $\zeta_S \in \mathbb{R}^+$ is a constant.

IV. STABILITY ANALYSIS

To perform stability analysis, we define $y(t) \in \mathcal{D} \subset \mathbb{R}^4$ as

$$y \triangleq \left[e_1, e_2, \sqrt{P}, \sqrt{Q} \right]^T, \tag{32}$$

where e_1 and e_2 are the error terms defined in (10) and (11), $P(v,t,\tau) \in \mathbb{R}$ and $Q(e_2,t,\tau) \in \mathbb{R}$ are LK functionals that were designed based on the subsequent stability analysis

$$P = \omega \int_{t-\tau}^{t} \left(\int_{s}^{t} v(\theta)^{2} d\theta \right) ds, \tag{33}$$

$$Q = \frac{\bar{\xi}J_2K}{2} \int_{t-\tau}^t e_2(\theta)^2 d\theta, \tag{34}$$

where $\omega \in \mathbb{R}^+$ is a known constant. These LK functionals are designed for delay compensation analysis and similar functional have been used in our previous studies [13], [14], [18], [42].

Theorem 1. The controller given in (13) ensures semi-global uniformly ultimately bounded (UUB) tracking

$$|y(t)| \le \epsilon_0 \exp(-\epsilon_1 t) + \epsilon_2,$$
 (35)

 $\epsilon_0, \epsilon_1, \epsilon_2 \in \mathbb{R}^+$ denotes constants, provided the control gains α, β , and K introduced in (11) and (13) are selected according to the sufficient conditions

$$\alpha > \frac{\beta^2 \gamma^2}{4},$$

$$K_3 > \omega K^2 \tau + 2\bar{\xi} J_2 K,$$
(36)

where the known positive constants β , $\bar{\xi}$, J_2 , K, K_3 , ω are defined in (11), (24), (22), (13), (14) and (33), respectively, τ is the input delay, and $\gamma \in \mathbb{R}^+$ is a subsequently defined constant

Proof: A positive definite Lyapunov functional candidate $V(y,t): \mathcal{D} \times [0 \infty) \to \mathbb{R}$ is defined as

$$V \triangleq \frac{1}{2}e_1^2 + \frac{1}{2}J_{\Omega}e_2^2 + P + Q,\tag{37}$$

and satisfies the following inequalities

$$\lambda_1 \|y\|^2 \le V \le \lambda_2 \|y\|^2, \tag{38}$$

where $\lambda_1, \ \lambda_2 \in \mathbb{R}^+$ are known constants.

Taking the time derivative of (37) and using the Leibniz integral rule to differentiate P and Q in (33) and (34), we get

$$\dot{V} = e_{1}\dot{e}_{1} + \frac{1}{2}\dot{J}_{\Omega}e_{2}^{2} + J_{\Omega}e_{2}\dot{e}_{2} + \frac{\xi J_{2}K}{2}\left(e_{2}^{2} - e_{2\tau}^{2}\right) (39)
+\omega\tau v^{2} - \omega \int_{t-\tau}^{t} v\left(\theta\right)^{2}d\theta
= -\alpha e_{1}^{2} + \beta e_{z}e_{1} + e_{2}\left[\bar{\psi} + \tilde{\psi} - KJ_{\Omega}\xi\left(e_{2} - e_{2\tau}\right)\right]
-Ke_{2} + \frac{\bar{\xi}J_{2}K}{2}\left(e_{2}^{2} - e_{2\tau}^{2}\right) + \omega\tau v^{2}
-\omega \int_{t-\tau}^{t} v\left(\theta\right)^{2}d\theta
\leq -\alpha e_{1}^{2} - (K + KJ_{\Omega}\xi)e_{2}^{2} + |e_{2}|\rho\left(||z||\right)||z||
+|e_{2}|\zeta_{s} + \beta|e_{1}||e_{z}| + KJ_{\Omega}\xi|e_{2\tau}||e_{2}|
+\frac{\bar{\xi}J_{2}K}{2}\left(e_{2}^{2} - e_{2\tau}^{2}\right) + \omega\tau v^{2} - \omega \int_{t-\tau}^{t} v\left(\theta\right)^{2}d\theta.$$

Applying Young's Inequality the following terms in (40) can be bounded as

$$\beta|e_1||e_z| \le \frac{\beta^2 \gamma^2}{4} e_1^2 + \frac{1}{\gamma^2} e_z^2,$$
 (41)

$$|e_{2\tau}||e_2| \le \frac{1}{2}e_{2\tau}^2 + \frac{1}{2}e_2^2,$$
 (42)

where $\gamma \in \mathbb{R}^+$ is a known constant that is selected as

$$\gamma > \sqrt{\frac{2\tau}{\omega}}.\tag{43}$$

Further, by using the Cauchy Schwartz inequality, the following term in (41) can be bounded as

$$e_z^2 \le \tau \int_{t-\tau}^t v(\theta)^2 d\theta. \tag{44}$$

After adding and subtracting $\frac{\tau}{\sqrt{2}}\int_{t-\tau}^{t}v\left(\theta\right)^{2}d\theta$ to (40) and utilizing (41), (42) and (44), (40) can be expressed as

$$\dot{V} \leq -\left(\alpha - \frac{\beta^{2} \gamma^{2}}{4}\right) e_{1}^{2} - \left(K - 2KJ_{2}\bar{\xi} - \omega K^{2}\tau\right) e_{2}^{2}
- \frac{1}{\tau} \left(\omega - \frac{2\tau}{\gamma^{2}}\right) e_{z}^{2} + |e_{2}|\rho\left(\|z\|\right) \|z\| + \zeta_{S}|e_{2}|
- \frac{\tau}{\gamma^{2}} \int_{1}^{t} v\left(\theta\right)^{2} d\theta.$$
(45)

By using (14), (30) and completing the squares, the inequality in (45) can be further upper bounded as

$$\dot{V} \leq -\left(\alpha - \frac{\beta^{2} \gamma^{2}}{4}\right) e_{1}^{2} - \left(K_{3} - 2KJ_{2}\bar{\xi} - \omega K^{2}\tau\right) e_{2}^{2}
- \frac{1}{\tau} \left(\omega - \frac{2\tau}{\gamma^{2}}\right) e_{z}^{2} + \left(|e_{2}|\rho\left(\|z\|\right)\|z\| - K_{1}e_{2}^{2}\right)
- \frac{\tau}{\gamma^{2}} \int_{t-\tau}^{t} v\left(\theta\right)^{2} d\theta + \left(\zeta_{S}|e_{2}| - K_{2}e_{2}^{2}\right)
\leq -\left\{\Lambda - \frac{\rho^{2}\left(\|z\|\right)}{4K_{1}}\right\} \|z\|^{2} - \frac{\tau}{\gamma^{2}} \int_{t-\tau}^{t} v\left(\theta\right)^{2} d\theta + \frac{\zeta_{S}^{2}}{4K_{2}},$$
(46)

where

$$\Lambda \triangleq \min \left[\alpha - \frac{\beta^2 \gamma^2}{4}, K_3 - \omega K^2 \tau - 2\bar{\xi} J_2 K, - \frac{1}{\tau} \left(\omega - \frac{2\tau}{\gamma^2} \right) \right].$$
(47)

Because

$$\int_{t-\tau}^{t} \left(\int_{s}^{t} v(\theta)^{2} d\theta \right) ds \le \tau \int_{t-\tau}^{t} v(\theta)^{2} d\theta, \tag{48}$$

after utilizing (33), (34) and (13)

$$-\frac{\tau}{2\gamma^2} \int_{t-\tau}^t v(\theta)^2 d\theta \leq -\frac{P}{\omega \gamma^2}$$
$$-\frac{\tau}{2\gamma^2} \int_{t-\tau}^t v(\theta)^2 d\theta \leq -\frac{K\tau}{\gamma^2 \bar{\xi} J_2} Q \tag{49}$$

the inequality in (46) can be rewritten as

$$\dot{V} \le -\left(\Lambda - \frac{\rho^2(\|z\|)}{4K_1}\right) \|z\|^2 - \frac{K\tau}{\gamma^2 \bar{\xi} J_2} Q \qquad (50)$$
$$-\frac{1}{2\omega\gamma^2} P + \frac{\zeta_S^2}{4K_2}.$$

Using the definition of z(t) in (30) and y(t) in (32), the expression in (50) can be upper bounded as

$$\dot{V} \le -\bar{\mu} \|y\|^2 - \left(\Lambda - \frac{\rho^2 (\|z\|)}{4K_1}\right) \|e_z\|^2 + \frac{\zeta_S^2}{4K_2},$$
 (51)

where $\bar{\mu}(||z||) \in \mathbb{R}^+$ is

$$\vartheta \leq \bar{\mu} \triangleq \min \left[\Lambda - \frac{\rho^2 \left(\|z\| \right)}{4K_1}, \ \frac{K\tau}{\gamma^2 \bar{\xi} J_2}, \ \frac{1}{2\omega \gamma^2} \right]$$

for some $\vartheta \in \mathbb{R}^+$. In order to further bound (51), $\Lambda - \frac{\rho^2(\|z\|)}{4K_1} > 0$ is required, which gives $\|z\|^2 < \rho^{-2} \left(2\sqrt{\Lambda K_1}\right)$. Consider a set S defined as

$$S \triangleq \left\{ y(t) \in R^{4} | \|y(0)\| < \sqrt{\frac{\lambda_{1}}{\lambda_{2}} \min\left\{1, \frac{2K\tau}{\bar{\xi}J_{2}}\right\} \rho^{-2} \left(2\sqrt{\Lambda K_{1}}\right) - \frac{\zeta_{S}^{2}}{4K_{2}\vartheta}} \right\},$$

$$(52)$$

By further utilizing (38), the inequality in (51) can be expressed as

$$\dot{V} \le -\frac{\vartheta}{\lambda_2} V + \frac{\zeta_S^2}{4K_2}.\tag{53}$$

The linear differential equation in (53) can be solved as

$$V \le V(0) e^{-\frac{\vartheta}{\lambda_2}t} + \frac{\zeta_S^2 \lambda_2}{4K_2 \vartheta} \left[1 - e^{-\frac{\vartheta}{\lambda_2}t} \right], \tag{54}$$

provided the control gains satisfied the sufficient conditions (36), the results (35) can be obtained from (54). Based on the definition of y(t), the results in (54) indicates that $e_1, e_2 \in \mathcal{L}_{\infty}$ in S.

Remark 1. EMD of antagonist muscles are generally different. The above stability analysis was performed using Assumption 3 that EMD of the antagonist muscles is known and the same. In our previous result, we have shown a PID-type delay compensating controller to be robust to an unknown delay value [43]. Using a similar stability analysis in [43], sufficient gain conditions can be derived to show that the proposed delay compensating controller in this paper is robust to different EMD values in the antagonistic muscles.

For implementation, the best way to apply the sufficient gain conditions is to use a known upper bound of the EMD if the delay value is uncertain. The control gain α performs like a proportional gain. α is related to γ , which is a known constant that can be selected based on the upper bound of EMD.

V. EXPERIMENTS

This study was approved by the Institutional Review Board (IRB) at the North Carolina State University (IRB approval number: 20575). Four participants without disabilities signed informed consent forms to participate. The study inclusion criteria were: 1) age of 18 - 40 years, 2) able to perform upper limb movements, and 3) able to perform movements with FES. The study exclusion criteria were: 1) persons with heart conditions, 2) absent sensation in upper limbs, 3) history of a neurological or an orthopedic condition that impairs normal upper limb movement, and 4) pregnant females.

The effectiveness of the switching controller was validated by controlling the FES input to the biceps and triceps of the four participants. A single joint one-degree of freedom elbow flexion and extension motion was performed in the horizontal plane, which can be seen in Fig. 1. The gravitational force was compensated by the SaeboMas Mini arm supporter. The participant was equipped with a wearable orthosis. The structure of the test bed is shown in Fig. 2. An incremental optical encoder (Hengxiang, CN) with 1024 pulses per revolution resolution was equipped onto the joint that measured the angle during the testing period. The control law was based on the error between the measured angle and the desired angle. A RehaStim 8-channel stimulator (Hasomed GmbH) was used to generate the current that was applied to the muscles. The current was set with 35 Hz and varying pulse widths for different participants. During the process, the participants were instructed to relax and avoid voluntary movement during the electrical stimulation. To avoid voluntary force by the participants, they were not allowed to view the desired and real trajectory at any time.

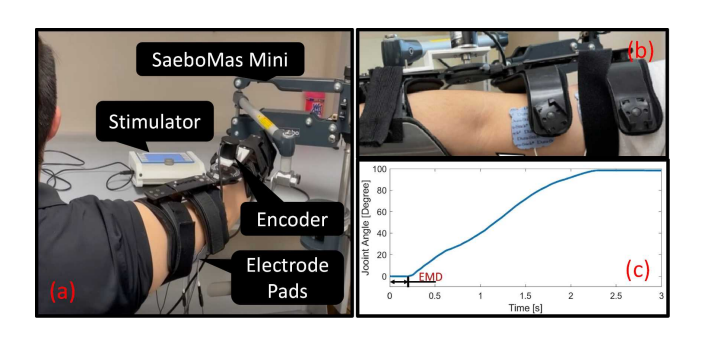


Figure 2. (a) An illustration of the test bed. The participants wore an arm orthosis that comprises of an arm orthosis and a SaeboMas Mini arm system. The arm orthosis spanned the elbow and had an encoder to measure the elbow angle. The SaeboMas Mini arm system was used for gravity compensation and for keeping the lower arm movement in the horizontal plane. (b) Zoomed in illustration of electrodes placement on the biceps muscle. (c) Experimental determination of an EMD value.

A. Experimental Determination of EMD Values

EMD values in the antagonist muscles were determined prior to the experiments. To identify the EMD τ , each participant wore the arm orthosis and was tested with a step input stimulation. As is seen in Fig. 2 (c), the delay in the arm movement was approximately assumed as the EMD. Each participant had three trials on both biceps and triceps and EMD

values were averaged and used in the controller. We used the pulse train with an amplitude of 10 mA, frequency of 20 Hz and pulse width with 80% of each subject's saturation level. The stimulation was designed with 3 seconds on and 2 seconds off repeated patterns, and we measured the EMD values by averaging all the EMDs along the experiment.

For the sake of curiosity, we also measured EMD values when an antagonistic muscle was co-activated. We performed additional experiments to verify whether the EMD would disappear during co-contraction. A stimulation intensity at 80% of the saturation value was chosen to stimulate the biceps and triceps muscles under these two conditions: when the antagonist muscle was not co-activated and when the antagonist muscle was co-activated at low stimulation values.

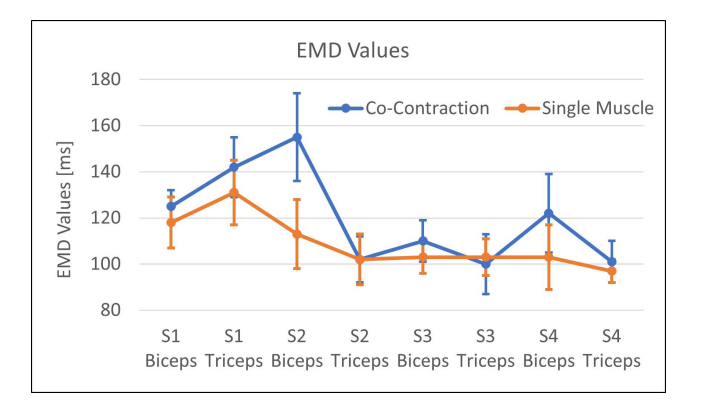


Figure 3. The averaged EMD with standard deviations for the biceps and triceps among the four participants.

EMD Values					
Participant ID	Muscle	EMD (ms)			
		Single Muscle	Co-activation		
S_1	Biceps	118±11	125±7		
	Triceps	131±14	142±13		
S_2	Biceps	113±15	155±19		
	Triceps	102±11	102±10		
S_3	Biceps	103±7	110±9		
	Triceps	103±8	100±13		
S_4	Biceps	103±14	122±17		
	Triceps	97±5	101±9		
Threshold and Saturation Values					
Participant ID	Muscle	Threshold (μs)	Saturation (μs)		
S_1	Biceps	160	420		
51	Triceps	170	450		
S_2	Biceps	150	430		
	Triceps	200	450		
S_3	Biceps	100	450		
	Triceps	120	450		
S_4	Biceps	100	410		
<i>5</i> 4	Triceps	90	390		

Table I

THE AVERAGED EMD WITH STANDARD DEVIATIONS, SATURATION AND THRESHOLD PULSE WIDTH FOR THE BICEPS AND TRICEPS AMONG THE FOUR PARTICIPANTS.

We measured EMD values in both conditions. The antagonist muscle was stimulated at a constant level that is the sum of 10% of its saturation level and its stimulation threshold.

Contrary to our hypothesis that EMD would disappear due to co-activation, we found the delay in the co-activation cases to be similar and even bigger than the no co-activation cases. The averaged EMD values with their standard deviations for the four participants are shown in Figure 3 and Table I. Our results show that EMD is indeed present even during co-contraction. Therefore, it would be important to consider during FES control of antagonistic muscles.

Remark 2. A common EMD value during FES-elicited stimulation could range between 60-150 ms [38], [44], [45]. Literature usually report different methods to measure delay such as FES-invoked EMG onset. Unlike in the EMG-based approach we used the time difference between the stimulation trigger and an observable finite angle change from the encoder. The methods employed to measure delay are more relevant for the control objective. The EMD values from our measurements are in the range of 97-131 ms for a single muscle, which are similar to the values reported in our previous papers [13], [14].

B. FES Threshold and Saturation Identification

As is shown in (17), a normalized input was used in the controller. Therefore, the saturation and threshold stimulation levels were identified for the participants. The threshold is the minimum current pulse width required to produce an increase in the muscle force and the saturation is the minimum current pulse width at which there is no considerable increase in force or a desired maximum force is achieved [12]. To identify the threshold and saturation values, a pulse train of FES with increasing pulse widths was applied to biceps and triceps separately. The elbow joint angle and filtered acceleration from the encoder were measured. The filtered acceleration was used as the surrogate of the generated force to identify the threshold and saturation values. The identification results are given in Table I.

C. Tracking Performance Results

After the identification of EMD and the threshold and saturation value for the biceps and triceps of different participants, the switching controller was tested on the participants. The control objective was to track a desired sinusoidal trajectory. The controller's performance was tested for a desired trajectory with a constant 4 second period and was repeated eight times during each test. Each participant was provided a rest time of 5 seconds between two testing cycles. The range of angle movement was between 0° to 60° and the testing duration of each trial was 32 seconds. Each participant had a one minute break between two adjacent trials. To compare the performance of the new switching controller, the same tests were performed on a classical PD controller with an ad hoc switched mapping (PD-A).

The PD-A control was designed as:

$$v = K(\alpha e_1 + \dot{e}_1) \stackrel{\triangle}{=} K e_{II}$$

where e_1 is in (10). An ad hoc switching function was designed based on the sign of e_{II} .

$$S_{1}\left(e_{II}\right) = \begin{cases} 1, & e_{II} > 0 \\ 0, & e_{II} < 0 \end{cases}, \ S_{2}\left(e_{II}\right) = \begin{cases} 0, & e_{II} > 0 \\ -1, & e_{II} < 0 \end{cases}$$

It follows the same stimulation normalization rules as in (16) and (17), but it did not consider the EMD.

A limitation of the experiments with FES on human participants is that the gain tuning procedure takes time and can be different from person to person. It may cause muscle fatigue and discomfort for participants during this procedure. To mitigate this issue, the controller was tuned on a separate day to find initial control gains that gave acceptable results. Then on a separate day, the experiments started with the identified initial gains, and the gains needed only minor tuning.

There are three control gains to be tuned: K is related to both proportional and differential gain, α is related to the proportional gain and β is related to the delay compensation. To tune the PD-A controller, K and β were firstly set to be zero and α was increased until the output elbow angle oscillated. Then K was gradually increased until the output was acceptably near its reference. For PD-A controller, the control gain β was not included. Then we tuned the PD-DC controller starting with the previous control gains. We gradually increased α to make the output oscillate and increased the delay compensation gain β to lower the overshoot. Finally gain K was increased to achieve a good tracking result. The overall gain tuning process lasted approximated 30 minutes.

The electrode placements may change during different visits. To minimize this effect, the position of the electrode pads were marked by a pen and the participants were asked not to wash them off. The second visit was carried out shortly after the first trial to make sure the markings were still present. To further confirm the position, the old positions were photographed and compared for the second visit.

Some experimental results can be found in Fig. 4. The results successfully illustrate the ability of the PD-DC switching controller to track the desired trajectory. The root mean square error (RMSE), the root mean square and the maximum steady state errors and averaged input to two antagonistic muscles of the four participants under two different control strategies are listed in Table II.

The root mean square errors (RMSEs) of the four subjects range from 6.31 degrees to 10.36 degrees. The steady-state error is defined as the error that occurs after 8 seconds of the trial. The maximum steady-state error is defined as the maximum absolute value of error during that time periods. The RMS steady-state errors range from 5.6 degrees to 9.58 degrees. Comparing to the PD-A controller, the RMSE, SSE and the maximum SSE of the PD-DC controller were reduced by 17.3%, 25.6% and 28.6%. A Shapiro-Wilk test demonstrated that the tracking error data were normally distributed. Therefore, we performed a paired Student's t-test to compare the PD-DC controller and classical PD controller. The p-value was determined less than 1e-5, which means the PD-DC controller has a statistically significantly smaller tracking error compared to the classical PD controller. Table II shows that the PD-DC controller decreased the error both in transient and steady state. This is an expected outcome that validates the PD-DC control performance.

D. Disturbance Rejection and Fatigue Experimental Results

To further illustrate the performance of the developed controller, experiments were also conducted to validate disturbance rejection. The elbow was first regulated to a desired angle and an external disturbance was applied to the participant's hand. The disturbance was bidirectional to test the controller's ability to reject the disturbance in both directions. This test result is shown in Fig. 5 and Table III. The disturbance was applied twice for both tasks. The disturbance was applied to the end effector, by an impulse torque from the tester to deviate the elbow angle from the steady state. The averaged settling time (5%) after disturbance is from 3.4 s to 4.2 s. In the case of disturbances, due to its ability to continuously engage both triceps and biceps muscles, the controller would enable immediate return to the desired holding position, irrespective of the direction of the disturbance. This bidirectional disturbance rejection ability is unlike a classical control design for a single arm extension control that would not be able to reject an extensor disturbance. This controller thus would allow a superior task regulation like maintaining the elbow joint in a certain pose; e.g., while holding an object.

We also extended the experimental time from 32 seconds to 2 minutes to test the control performance in muscle fatiguing conditions. The tracking results and the inputs to the muscles are shown in Fig. 6 and Table IV. From this figure, we can see the controller can track the desired trajectory well for the first 70 seconds. We consider that during this time duration, the muscles may not have fatigued. The RMSE during this time period is 6.68 degrees. The controller can be applied to unfatigued muscles to generate continuous bidirectional motion with the ability to reject bidirectional impulse disturbance. However, after 70 seconds, the maximum angle could not reach the desired angle because of the muscle fatigue and follows a decaying trend. Therefore, the input plot shows that more stimulation was applied to the muscles to decrease the error. After muscles became fatigue, the averaged biceps and triceps muscle input was increased by 158% and 75% respectively. The overall RMSE was increased by 130%. This switching controller uses a high gain algorithm to obtain a fast transition rate and less overshoot during the tracking. Thus, the controller ineffectively deals the muscle fatigue-induced effects.

	Settling Time [s]	Mean Settling Time After Disturbance [s]
No Disturbance	7.9	N/A
Flexor Disturbance	8.3	3.4
Extensor Disturbance	6.3	4.2

Table III SETTLING TIME AFTER A DISTURBANCE TO THE SUBJECT'S HAND

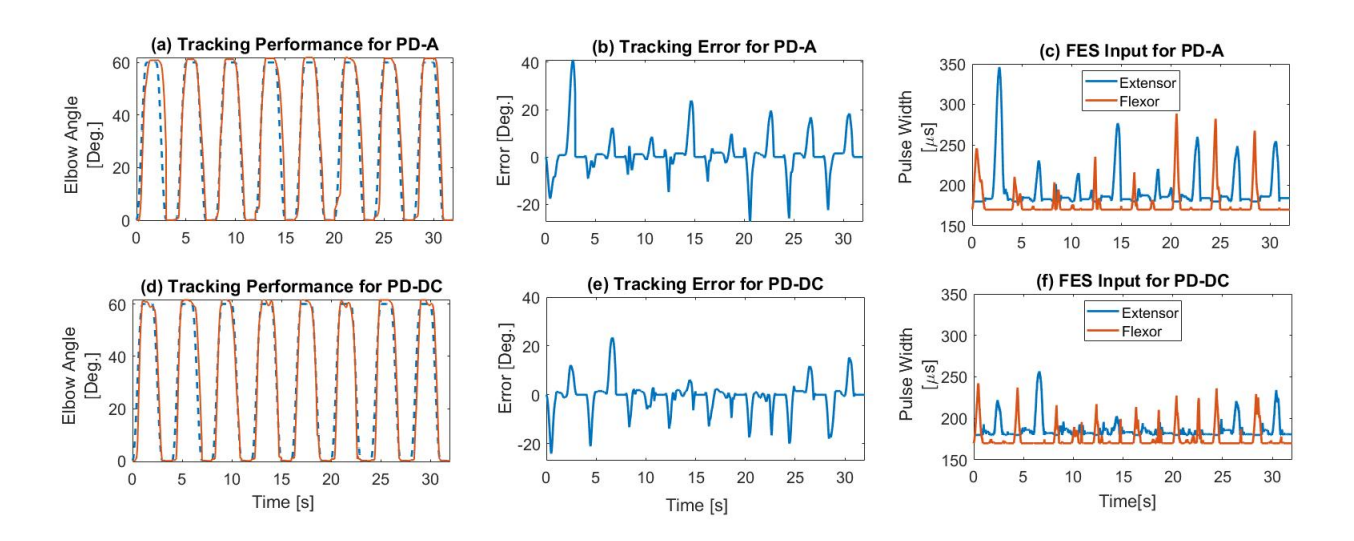


Figure 4. This figure shows the control performance for subject 1 under two different controllers, PD-A controller (top plot) and the PD-DC switching controller (bottom plot). The left two figures show the elbow angle during the control. (a) Tracking performance for PD-A; (d) Tracking performance for PD-DC. The dashed blue curve is represented for the desired trajectory and the solid red curve is represented for the real trajectory. The middle two figures show the tracking errors. (b) Tracking error for PD-A; (e) Tracking error for PD-DC. The two right figures are the FES pulse widths for biceps (red) and triceps (blue) muscles. (c) FES input (pulse width) for PD-A; (f) FES input (pulse width) for PD-DC.

Subject ID	RMSE [Deg.]		SSE [Deg.]		Max SSE [Deg.]	
Subject ID	PD-A	PD-DC	PD-A	PD-DC	PD-A	PD-DC
S_1	8.28±1.96	6.31 ± 0.99	7.72 ± 1.68	5.6 ± 0.87	23.81 ± 2.77	15.31±1.01
S_2	10.36 ± 2.09	$8.92{\pm}1.88$	8.43±2.00	5.94 ± 1.28	25.94 ± 2.75	14.88 ± 1.53
S_3	9.93±1.01	9.59 ± 0.81	8.78±1.78	6.53 ± 1.26	27.46 ± 3.22	22.83±3.75
S_4	10.70 ± 2.32	7.65 ± 1.21	9.58 ± 1.86	7.61 ± 1.53	26.65 ± 2.91	21.28±3.82
Average	9.81±1.85	8.11 ± 1.22	8.63±1.83	6.42 ± 1.23	26 ± 2.91	18.57 ± 2.53

Table II

THIS TABLE SHOWS THE RMSE, STEADY STATE ERROR (SSE) AND THE MAXIMUM SSE WITH STANDARD DEVIATIONS FOR EACH PARTICIPANT AS WELL AS THE AVERAGED RESULTS. PD-A REFERS TO THE AD HOC PD CONTROLLER, AND PD-DC REFERS TO THE PD CONTROLLER WITH A DELAY COMPENSATOR, WHICH IS DESIGNED IN THIS PAPER.

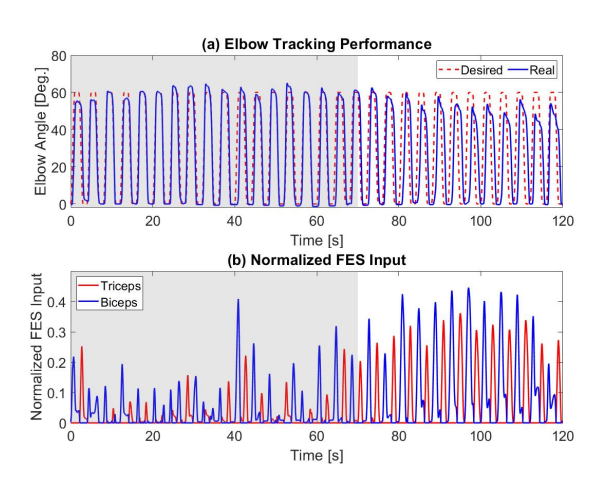


Figure 6. (a) Tracking performance and (b) the normalized FES input of the 2-minute test. The shaded area means that the muscles were not yet fatigued.

	Before Fatigue	During Fatigue	Entire Duration
RMSE [Deg.]	6.68	27.4	15.34
Mean u_e	0.12	0.21	0.16
Mean u_f	0.14	0.33	0.22

 $\label{thm:local_transform} \text{Table IV}$ The control performance in the 2-minute experiment

VI. DISCUSSION AND CONCLUSION

In this paper, a novel FES switching controller with input delay compensation for antagonistic muscles was designed. The controller provided an arbitrary short transition period when two antagonistic muscles were simultaneously activated to ensure that there were no discontinuities in muscle response so that the elbow could flex and extend smoothly. A Lyapunov-Krasovskii functional was used to prove that the developed controller yields ultimately bounded tracking of a desired trajectory provided the control gains satisfied sufficient conditions. The experiments were conducted on four participants without disabilities. Experimental results indicate that the controller is robust and could switch between opposing muscles without affecting the tracking performance and UUB tracking was realized during the experiments. Comparing to the ad-hoc switching controller, the new controller obtained a statistically significant reduction in the tracking RMSE. The

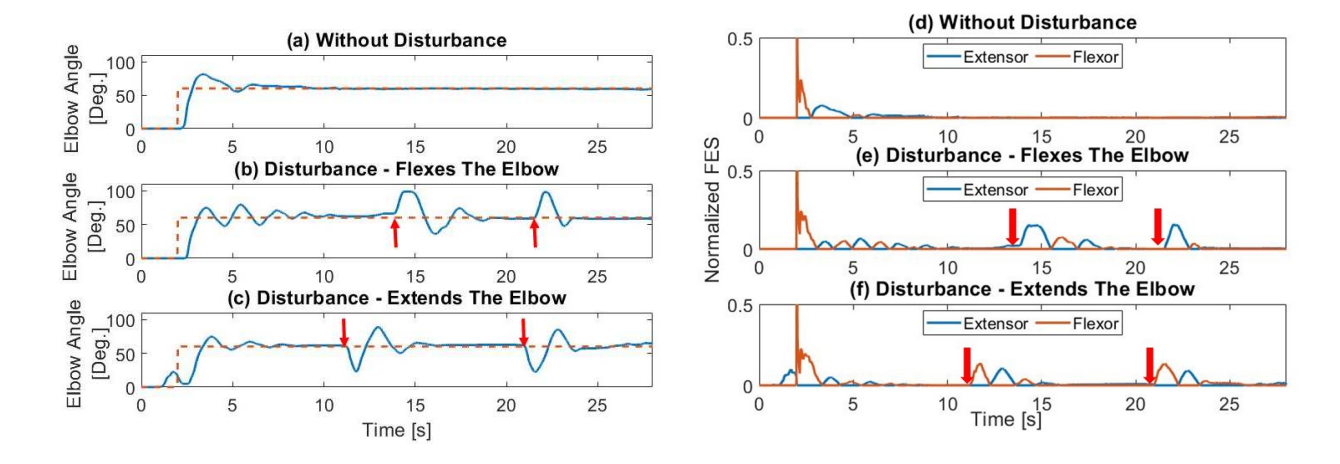


Figure 5. This figure shows the controller's ability to reject the disturbance from both directions. The desired trajectory (red dashed) is a step function with an amplitude of 60°. The tracking performance is represented in solid blue curve. The red arrows show when the impulse disturbance was applied to the subject. Figure (a) is the regulation task without disturbance. Figure (b) has a disturbance that flexed the elbow. Figure (c) has a disturbance that extended the elbow. Figures (d) - (f) show the FES input of these three cases.

controller can thus be applied to horizontal reaching tasks. The controller showed the ability to reject the disturbance from both directions. This means it can be used in people with paralyzed or weak antagonistic muscles. However, a limitation of this controller is that if lower motor neurons that control a particular joint are damaged for any reason, FES may not be a feasible way to control the joint. Future work will explore new analysis methods that allow for optimal adaptive controllers to be included in the switching design and also compensate for the muscle fatigue. We will also include the muscle fatigue model and consider the fatigue effect in the muscle activation function. FES control approaches in [12], [18], [43] can extend the designed FES controller in this paper to compensate for additional fatigue, muscle activation, and unknown EMD in the dynamics. Separately, we also showed that EMD values were not significantly reduced by adding co-activation to the muscles compared to stimulating a single muscle during the experiment. Notably, other works on co-activated muscles [11], [28], [29], [46] did not explicitly determined if EMD would disappear due to co-activation. Our study shows that the EMDs are indeed present in the co-activated muscle pair of people with no disabilities. However, people with disabilities were not involved in our study. It is possible that due to spastic muscles or impaired proprioception, coactivated muscles of individuals with disabilities may have additional or diminished effects of EMD. In the future, we will investigate how in people with disabilities, co-activation of muscles affects EMD. We also noted that EMD of two different muscles may be slightly different in measurement or may be time-varying during the experiments. Future work will include compensation for time-varying unknown delays and experiments will be performed on subjects with SCI. Further we would consider including new muscle recruitment models, e.g. in [11], and using the control methodology in [18] to include the muscle activation dynamics in our future work on antagonistic muscle control.

REFERENCES

- The National SCI Statistical Center, 515 Spain Rehabilitation Center 1717 6th Avenue South Birmingham, AL 35233-7330, "Spinal cord injury (SCI) facts and figures at a glance," 2019.
- [2] P. H. Peckham and J. S. Knutson, "Functional electrical stimulation for neuromuscular applications," *Annu. Rev. Biomed. Eng.*, vol. 7, pp. 327– 360, 2005.
- [3] E. K. Chadwick, D. Blana, J. D. Simeral, J. Lambrecht, S. P. Kim, A. S. Cornwell, D. M. Taylor, L. R. Hochberg, J. P. Donoghue, and R. F. Kirsch, "Continuous neuronal ensemble control of simulated arm reaching by a human with tetraplegia," *J. Neural Eng.*, vol. 8, no. 3, p. 034003, 2011.
- [4] E. Schearer, Y.-W. Liao, E. Perreault, M. Tresch, W. Memberg, R. Kirsch, and K. Lynch, "Multi-muscle FES force control of the human arm for arbitrary goals," *IEEE Trans. Neural Syst. Rehabil. Eng.*, vol. 22, no. 3, pp. 654–663, 2014.
- [5] M. K. Nagai, C. Marquez-Chin, and M. R. Popovic, "Why is functional electrical stimulation therapy capable of restoring motor function following severe injury to the central nervous system?" in *Translational Neuroscience*. Springer, 2016, pp. 479–498.
- [6] F. Previdi, M. Ferrarin, S. M. Savaresi, and S. Bittanti, "Gain scheduling control of functional electrical stimulation for assisted standing up and sitting down in paraplegia: a simulation study," *Int. J. Adapt. Control Signal Process.*, vol. 19, pp. 327–338, 2005.
- [7] H. Gollee, K. J. Hunt, and D. E. Wood, "New results in feedback control of unsupported standing in paraplegia," *IEEE Trans. Neural Syst. Rehabil. Eng.*, vol. 12, no.1, pp. 73–91, 2004.
- [8] K. J. Hunt and M. Munih., "Feedback control of unsupported standing in paraplegia-part 1: Optimal control approach," *IEEE Trans. Rehabil. Eng.*, vol. 5, pp. 331–340, 1997.
- [9] N. Sharma, K. Stegath, C. M. Gregory, and W. E. Dixon, "Nonlinear neuromuscular electrical stimulation tracking control of a human limb," *IEEE Trans. Neural Syst. Rehabil. Eng.*, vol. 17, no. 6, pp. 576–584, 2009.
- [10] N. Sharma, C. Gregory, M. Johnson, and W. Dixon, "Closed-loop neural network-based NMES control for human limb tracking," *IEEE Trans. Control Syst. Technol.*, vol. 20, no. 3, pp. 712–725, 2012.
- [11] A. P. L. Bo, L. O. da Fonseca, and A. C. C. de Sousa, "Fes-induced coactivation of antagonist muscles for upper limb control and disturbance rejection," *Medical engineering & physics*, vol. 38, no. 11, pp. 1176– 1184, 2016.
- [12] N. Sharma, N. A. Kirsch, N. A. Alibeji, and W. E. Dixon, "A non-linear control method to compensate for muscle fatigue during neuromuscular electrical stimulation," *Frontiers in Robotics and AI*, vol. 4, p. 68, 2017.
- [13] N. Alibeji, N. Kirsch, S. Farrokhi, and N. Sharma, "Further results on predictor-based control of neuromuscular electrical stimulation," *IEEE Trans. Neural Syst. Rehabil. Eng.*, 2015.

- [14] N. Sharma, C. Gregory, and W. E. Dixon, "Predictor-based compensation for electromechanical delay during neuromuscular electrical stimulation," *IEEE Trans. Neural Syst. Rehabil. Eng.*, vol. 19, no. 6, pp. 601– 611, 2011.
- [15] S. Obuz, V. H. Duenas, R. J. Downey, J. R. Klotz, and W. E. Dixon, "Closed-loop neuromuscular electrical stimulation method provides robustness to unknown time-varying input delay in muscle dynamics," *IEEE Trans. Control Syst. Technol.*, 2019.
- [16] T. Schauer, N. O. Negard, F. Previdi, K. J. Hunt, M. H. Fraser, E. Ferchland, and J. Raisch, "Online identification and nonlinear control of the electrically stimulated quadriceps muscle," *Control Eng. Pract.*, vol. 13, pp. 1207–1219, 2005.
- [17] S. Jezernik, R. G. Wassink, and T. Keller, "Sliding mode closed-loop control of FES controlling the shank movement," *IEEE Trans. Biomed. Eng.*, vol. 51, no. 2, pp. 263–272, 2004.
- [18] N. Alibeji, N. Kirsch, B. E. Dicianno, and N. Sharma, "A modified dynamic surface controller for delayed neuromuscular electrical stimulation," *IEEE/ASME Trans. Mechatronics*, vol. 22, no. 4, pp. 1755–1764, Aug 2017.
- [19] I. Karafyllis, M. Malisoff, M. de Queiroz, M. Krstic, and R. Yang, "Predictor-based tracking for neuromuscular electrical stimulation," *Int. J. Robust Nonlinear Control*, vol. 25, no. 14, pp. 2391–2419, 2015.
- [20] W. K. Durfee and K. E. MACLean, "Methods for estimating isometric recruitment curves of electrically stimulated muscle," *IEEE Trans. Biomed. Eng.*, vol. 36, no. 7, pp. 654–667, 1989.
- [21] K. Masani, A. H. Vette, N. Kawashima, and M. R. Popovic, "Neuromusculoskeletal torque-generation process has a large destabilizing effect on the control mechanism of quiet standing," *J. Neurophysiol.*, vol. 100, no. 3, p. 1465, 2008.
- [22] M. Merad, R. J. Downey, S. Obuz, and W. E. Dixon, "Isometric torque control for neuromuscular electrical stimulation with time-varying input delay," *IEEE Trans. Control Syst. Technol.*, 2015.
- [23] J. P. Giuffrida and P. E. Crago, "Functional restoration of elbow extension after spinal-cord injury using a neural network-based synergistic FES controller," *IEEE Trans. Neural Syst. Rehabil. Eng.*, vol. 13, no. 2, pp. 147–152, 2005.
- [24] K. L. Meadmore, T. A. Exell, E. Hallewell, A.-M. Hughes, C. T. Freeman, M. Kutlu, V. Benson, E. Rogers, and J. H. Burridge, "The application of precisely controlled functional electrical stimulation to the shoulder, elbow and wrist for upper limb stroke rehabilitation: a feasibility study," *J NeuroEng Rehabil*, vol. 11, no. 1, p. 105, 2014.
- [25] P. Sampson, C. Freeman, S. Coote, S. Demain, P. Feys, K. Meadmore, and A.-M. Hughes, "Using functional electrical stimulation mediated by iterative learning control and robotics to improve arm movement for people with multiple sclerosis," *IEEE Trans. Neural Syst. Rehabil. Eng.*, vol. 24, no. 2, pp. 235–248, 2015.
- [26] C. T. Freeman, A.-M. Hughes, J. H. Burridge, P. H. Chappell, P. L. Lewin, and E. Rogers, "A model of the upper extremity using FES for stroke rehabilitation," *J Biomech Eng*, vol. 131, no. 3, p. 031011, 2009.
- [27] C. Freeman, D. Tong, K. Meadmore, A. Hughes, E. Rogers, and J. Burridge, "FES based rehabilitation of the upper limb using input/output linearization and ILC," in *IEEE ACC, Montreal, QC, Canada*. IEEE, 2012, pp. 4825–4830.
- [28] C. Klauer, J. Raisch, and T. Schauer, "Nonlinear joint-angle feedback control of electrically stimulated and λ-controlled antagonistic muscle pairs," in 2013 European Control Conference (ECC). IEEE, 2013, pp. 3101–3107.
- [29] E. H. Copur, C. T. Freeman, B. Chu, and D. S. Laila, "Repetitive control of electrical stimulation for tremor suppression," *IEEE Trans. Control* Syst. Technol., vol. 27, no. 2, pp. 540–552, 2017.
- [30] M. J. Dolan, B. J. Andrews, and P. Veltink, "Switching curve controller for fes-assisted standing up and sitting down," *IEEE Trans. Rehabil. Eng.*, vol. 6, no. 2, pp. 167–171, 1998.
- [31] C. Wiesener and T. Schauer, "The cybathlon rehabike: Inertial-sensor-driven functional electrical stimulation cycling by team hasomed," *IEEE Robotics & Automation Magazine*, vol. 24, no. 4, pp. 49–57, 2017.
- [32] A. P. Bo, L. O. da Fonseca, J. A. Guimaraes, E. Fachin-Martins, M. E. Paredes, G. A. Brindeiro, A. C. C. de Sousa, M. C. Dorado, and F. M. Ramos, "Cycling with spinal cord injury: A novel system for cycling using electrical stimulation for individuals with paraplegia, and preparation for cybathlon 2016," *IEEE Robotics & Automation Magazine*, vol. 24, no. 4, pp. 58–65, 2017.
- [33] R. J. Downey, T.-H. Cheng, M. J. Bellman, and W. E. Dixon, "Closed-loop asynchronous neuromuscular electrical stimulation prolongs functional movements in the lower body," *IEEE Trans. on Neural Syst. and Rehabil. Eng.*, vol. 23, no. 6, pp. 1117–1127, 2015.

- [34] T. Qiu, N. Alibeji, and N. Sharma, "Robust compensation of electromechanical delay during neuromuscular electrical stimulation of antagonistic muscles," in *American Control Conference (ACC)*, 2016. IEEE, 2016, pp. 4871–4876.
- [35] R. Riener and T. Fuhr, "Patient-driven control of FES-supported standing up: A simulation study," *IEEE Trans. Rehabil. Eng.*, vol. 6, pp. 113–124, 1998.
- [36] H. Hatze, "A myocybernetic control model of skeletal muscle," *Biological Cybernetics*, vol. 25, no. 2, pp. 103–119, 1977.
- [37] R. Happee, "Inverse dynamic optimization including muscular dynamics, a new simulation method applied to goal directed movements," J. Biomech., vol. 27, no. 7, pp. 953–960, 1994.
- [38] R. J. Downey, M. Merad, E. J. Gonzalez, and W. E. Dixon, "The time-varying nature of electromechanical delay and muscle control effectiveness in response to stimulation-induced fatigue," *IEEE Trans.* on Neural Syst. and Rehabil. Eng., 2016.
- [39] S. A. Binder-Macleod, J. C. Dean, and J. Ding, "Electrical stimulation factors in potentiation of human quadriceps femoris," *Muscle & nerve*, vol. 25, no. 2, pp. 271–279, 2002.
- [40] B. D. Doll, N. A. Kirsch, X. Bao, B. E. Dicianno, and N. Sharma, "Dynamic optimization of stimulation frequency to reduce isometric muscle fatigue using a modified hill-huxley model," *Muscle & nerve*, vol. 57, no. 4, pp. 634–641, 2018.
- [41] D. Popović, R. Stein, M. Oğuztöreli, M. Lebiedowska, and S. Jonić, "Optimal control of walking with functional electrical stimulation: a computer simulation study," *IEEE Trans. Rehabil. Eng.*, vol. 7, no. 1, pp. 69–79, 1999.
- [42] N. Sharma, S. Bhasin, Q. Wang, and W. E. Dixon, "Predictor-based control for an uncertain euler-lagrange system with input delay," *Automatica*, vol. 47, no. 11, pp. 2332–2342, 2011.
- [43] N. Alibeji and N. Sharma, "A PID-type robust input delay compensation method for uncertain euler-lagrange systems," *IEEE Trans. Control Syst. Technol.*, vol. 25, no. 6, pp. 2235–2242, 2017.
- [44] P. Cavanagh and P. Komi, "Electromechanical delay in human skeletal muscle under concentric and eccentric contractions," Eur. J. Appl. Physiol. Occup. Physiol., vol. 42, no. 3, pp. 159–163, 1979.
- [45] S. Zhou, D. L. Lawson, W. E. Morrison, and I. Fairweather, "Electrome-chanical delay in isometric muscle contractions evoked by voluntary, reflex and electrical stimulation," Eur. J. Appl. Physiol. Occup. Physiol., vol. 70, no. 2, pp. 138–145, 1995.
- [46] N. M. Oomen, N. P. Reeves, M. C. Priess, and J. H. van Dieën, "Trunk muscle coactivation is tuned to changes in task dynamics to improve responsiveness in a seated balance task," *Journal of Electromyography* and Kinesiology, vol. 25, no. 5, pp. 765–772, 2015.